Lab on a Chip

Accepted Manuscript

This is an *Accepted Manuscript*, which has been through the Royal Society of Chemistry peer review process and has been accepted for publication.

Accepted Manuscripts are published online shortly after acceptance, before technical editing, formatting and proof reading. Using this free service, authors can make their results available to the community, in citable form, before we publish the edited article. We will replace this *Accepted Manuscript* with the edited and formatted *Advance Article* as soon as it is available.

You can find more information about *Accepted Manuscripts* in the Information for Authors.

Please note that technical editing may introduce minor changes to the text and/or graphics, which may alter content. The journal's standard Terms & Conditions and the Ethical guidelines still apply. In no event shall the Royal Society of Chemistry be held responsible for any errors or omissions in this *Accepted Manuscript* or any consequences arising from the use of any information it contains.

ROYAL SOCIETY OF CHEMISTRY

www.rsc.org/loc

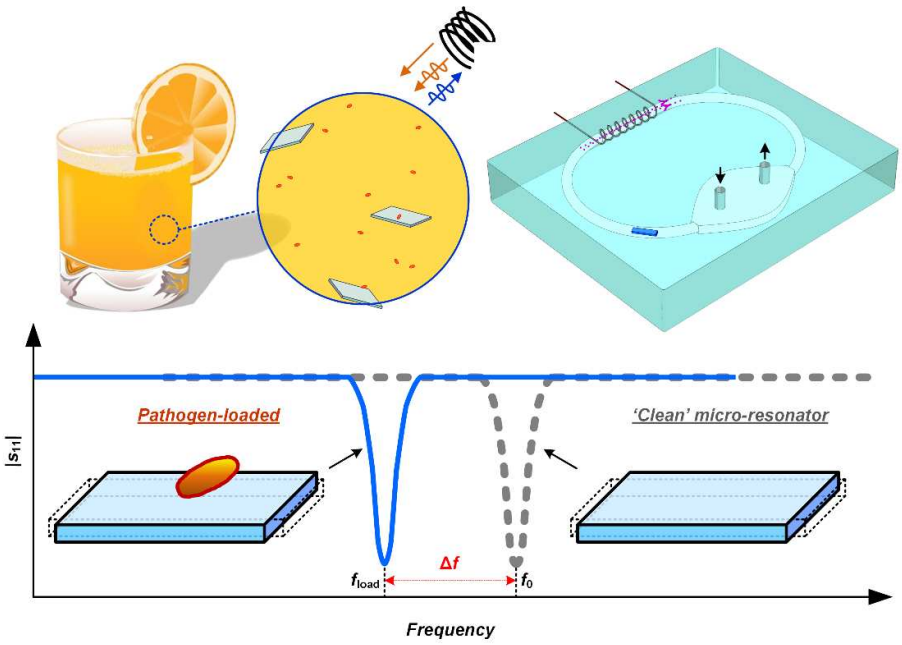

A wireless biosensing microfluidic-chip based on resonating 'μ-diver'

A magneto-elastic resonant 'micro-diver' system (MER-μDS) is proposed and developed for rapid liquid-phase detection of pathogen in wireless way.

Lab on a Chip Accepted Manuscript

Lab on a Chip

RSCPublishing

PAPER

A wireless biosensing microfluidic-chip based on resonating 'μ-diver'

Cite this: DOI: 10.1039/x0xx00000x

Cong Xue,[a] Chen Yang,[a] Tiegang Xu,[a] Jing Zhan [a] and Xinxin Li [a,*]

Received 00th January 2012,
Accepted 00th January 2012

DOI: 10.1039/x0xx00000x

www.rsc.org/

A magneto-elastic resonant 'micro-diver' system (MER-μDS) is proposed and developed for rapid liquid-phase detection of pathogen in wireless way. The magneto-elastic micro-resonator (i.e., the μ-diver) is put in the micro-chamber of the MER-μDS that is connected with the inlet/outlet for flow of liquid analyte and a close-looped micro-channel. After specific attachment of the analyte onto the μ-diver, the μ-diver is conveyed with flow into the detection segment of the channel, around which a metal micro-coil is wound for both exciting resonance of the μ-diver and reading its resonance-frequency signal. After the pre-functionalized μ-diver captures the analyte and, then, is driven to the detection channel-segment, the added mass induced resonant frequency shift can be wirelessly sensed by the coil. The micro-system features rapid and repeatable liquid-phase bio-sensing and the wireless signal readout scheme is favorable in real-time pathogen detection in liquid food, e.g., milk or juice, for food-safety applications. An equivalent-circuit model is established for design of the magneto-elastic μ-diver. After a bar-shaped μ-diver with length-extensional bulk-resonance mode is optimally designed and micro-fabricated, the MER-μDS is formed by micro-machining/assembling techniques. By putting a biotin-immobilized μ-diver in the wireless micro-sensing system, avidin-attached magnetic-beads are detected to calibrate the mass sensitivity as 0.061Hz pg^{-1}, which well confirms the modeling result. With the antibody-immobilized μ-diver, *E. coli* PBS-solution of 10^2~10^8 CFU mL^{-1} is detected, resulting in corresponding wireless f_0-shift sensing-signal as about 300~2300Hz and the limit of detection as 10^2 CFU mL^{-1}. Food-safety application potential of the MER-μDS technique is proved by detection of the *E. coli* added orange and apple juices (*E. coli* concentration: 10^4~10^8 CFU mL^{-1}).

Introduction

Lab-on-a-chip (LOC) systems and microfluidic technologies have the potential to enable much faster on-the-spot detection than conventional laboratory analysis and, thus, intensively attract research interests.[1-3] Among the biological techniques, rapid sensing methods[4-6] for on-site detection of microbiological objects, e.g., the pathogen of *E. coli* or *Salmonella* in solution, are highly demanded in the application fields like food safety[7,8], environment protection[9] and public health[10]. Among the developed biological detection schemes, magnetic phenomenon has already been utilized that includes magnetic resonance imaging (MRI),[11] biomagnetic separation[12,13] and magnetic immunoassay.[14] As for magnetic sensor techniques, magneto-elastic (ME) materials, which had ever been used in sonar systems and wireless motors [15-18], are recently experimentally proposed for resonance-type micro-sensors.[19,20] When the targeted bio-substance is bound onto the pre-functionalized surface of the tiny ME resonator, the specific mass attachment induces shift of the resonant frequency. In order to quickly detect the whole surface of solid food, e.g., apple, or liquid food, like milk or juice, a great number of such ME micro-resonators can be bestrewed to the food to recognize a small number of pathogens. Such a detection scheme is illustrated in Fig. 1. Besides the advantage of large vibrating amplitude and high resonance quality-factor (Q value), the ME resonant sensor features a unique nature of non-contact wireless excitation/sensing. This wireless sensing device is in contrast to the conventional surface-acoustic-wave (SAW) resonators[21,22], quartz-crystal-microbalance (QCM) sensors[23-25] or micro-cantilever sensors[26-28], where direct electrical interconnection is

[a] *State Key Lab of Transducer Technology, Shanghai Institute of Microsystem and Information Technology, Chinese Academy of Sciences, 865 Changning Road, Shanghai 200050, China. *E-mail: xxli@mail.sim.ac.cn; Fax: +86 21 62513510; Tel: +86 21 62131794*

Lab on a Chip Accepted Manuscript

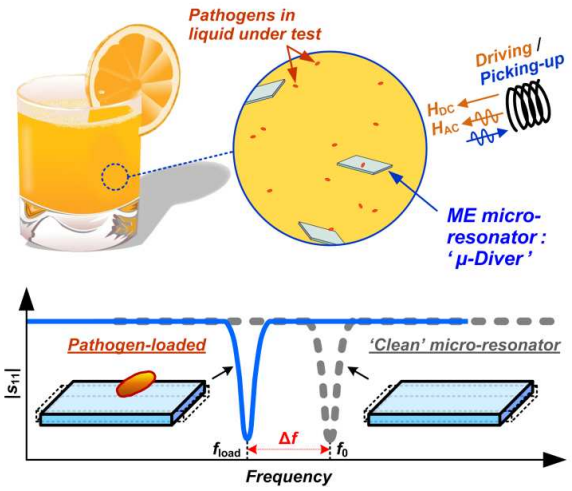

Fig. 1 Wireless bio-sensing scheme with magneto-elastic micro-resonators. The pathogen concentration is detected by measuring the resonance-peak shift (Δ*f*) *due to* mass change from 'clean' to pathogen-attached status.

always needed for resonance excitation and sensing signal readout.

Unfortunately, our calculation and experiment have indicated that the electromagnetic frequency-signal from the very tiny ME resonators are too weak to be measured by the wireless receiving coil when it is laid a bit far from the sensing resonators. The limited strength of the wireless electromagnetic signal hinders direct application of the ME resonators in practical detection.

In fact, the ME resonator features another inherent advantage. Being different from the root-clamped resonant cantilever biosensor whose structure has to be fixed in a bio-sensing chamber, the ME resonant bar can freely move in a micro-fluidic space to find and capture the targeted analyte. Naturally we hope to put the ME resonant bar into a micro-fluidic system for swimming and wireless bio-sensing. So far however, effort has seldom been made on integrated ME-resonator micro-systems like micro-fluidic lab-on-a-chip. For the first time, this study presents a lab-chip type ME resonant 'μ-diver' system (MER-μDS) that features three technical novelties: (1) integrated platform with repeatedly usable micro-resonator, namely, 'μ-diver'; (2) rapid operation mode for pathogen detection in liquid phase; (3) new equivalent-circuit modeling for optimal design of the MER-μDS towards ultra-sensitive bio-sensing applications.

The working scheme of the resonant μ-diver can be referred to the bottom plot in Fig. 1. Made of magnetostrictive material, the resonant μ-diver is immersed in pathogen liquid. When excited by an in-plane AC magnetic field (H_{AC}) from the excitation/test coil, the micro-resonator starts to vibrate due to magneto-striction effect. Herein a bias field (H_{DC}) from a bulk permanent magnet is superimposed to the AC field. When the biological species are specifically attached to the surface of the pre-modified μ-diver, the sensing signal is obtained by wireless measuring its resonant frequency shift. In fact, the mass addition dampens resonating behavior of the resonant sensor.[29]

The frequency f_0 of the length-extensional mode of the bar-shaped resonator depends on the length L, elasticity E, density ρ and Poisson's ratio v of the thick film resonator, η_{liq} and ρ_{liq} are the dynamic viscosity and density of the liquid as[30-33]

$$\begin{cases} f_0 = \dfrac{1}{2L}\sqrt{\dfrac{E}{\rho\left(1-v^2\right)}} = f_{air}\ (\text{in air})\ \text{or} \\ f_0 = f_{air} - \dfrac{\sqrt{\eta_{liq}\rho_{liq}/\pi}}{2\rho d}\cdot\sqrt{f_{air}}\ (\text{in low viscosity liquid}), \end{cases} \quad (1)$$

When the loaded mass of Δm is much smaller than the mass of the resonator M, the resonant-frequency shift of Δf can be deduced from Eq. (1) into following form of

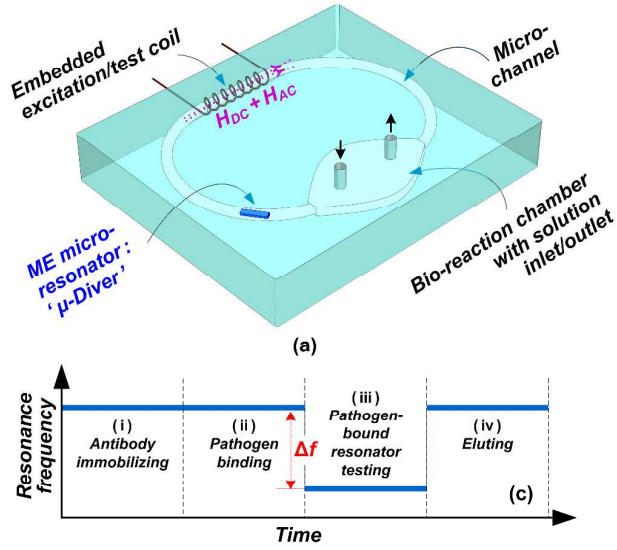

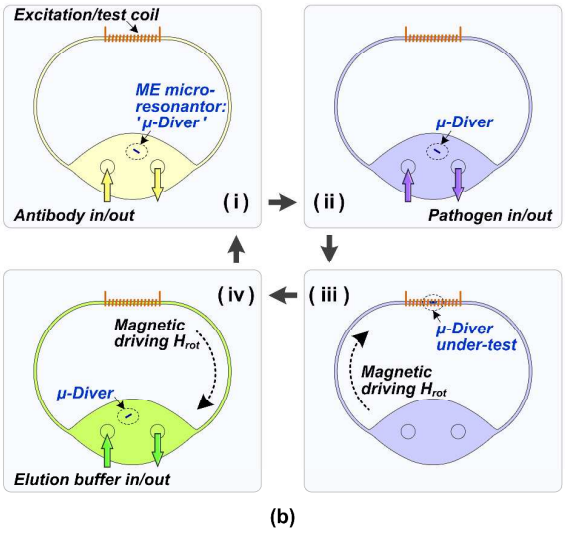

Fig. 2 (a) Schematic of the LOC type magneto-elastic resonant 'μ-diver' system (MER-μDS) for on-site pathogen detection in liquid. (b) Schematic four-step bio-detection procedure with the MER-μDS. (c) Demonstrated frequency-shift of the resonant μ-diver during the four steps.

Lab on a Chip Accepted Manuscript

This journal is © The Royal Society of Chemistry 2014

$$\Delta f = f_{\text{load}} - f_0 = -\frac{5f_0 - 3f_{\text{air}}}{4M} \cdot \Delta m \quad (2)$$

The detailed design of the system, modeling of the ME resonator, micro-fabrication and bio-sensing experiments will be addressed in following sections.

Design and modeling

Design of the bio-sensing system

The MER-μDS sensing micro-platform sketched in Fig. 2(a) is composed of a biological reaction chamber, a close-looped microfluidic channel, an embedded excitation/test coil winding around the channel and an inside laid ME μ-diver that can be driven (by external magnetic force) to swim around in the microfluidic channel. After the μ-diver is driven into the test coil, a frequency-sweeping excitation field (H_{DC} biased H_{AC}) is generated from the coil. With the wireless excitation, the μ-diver turns to resonate at its bulk acoustic-wave mode frequency of f_0 due to magneto-striction effect. Wirelessly tracked with the same coil, the f_0 signal is picked up as a negative peak in the reflection-coefficient $|s_{11}|$ spectrum. Corresponding to the mass change from the 'clean' state to the pathogen-loaded state, the shift of f_0 can be read out and, thus, the concentration of the pathogen analyte can be detected in real-time.

The repeatable pathogen detection procedure in the MER-μDS is schematically shown in Fig. 2(b) that includes: (i) immobilize the antibody on the surface of the μ-diver in the bio-reaction chamber; (ii) input pathogen solution for specific binding; (iii) frequency measurement by driving the μ-diver into the excitation/test coil via an externally rotating magnet (H_{rot}); and (iv) after detection, the μ-diver is driven back to the chamber for eluting and next-time repeated detection. The relationship between time and resonance frequency at these four steps is schematically sketched in Fig. 2(c). Besides the case of single μ-diver in the chamber, more resonators can be simultaneously put in for parallel capturing and serial detection.

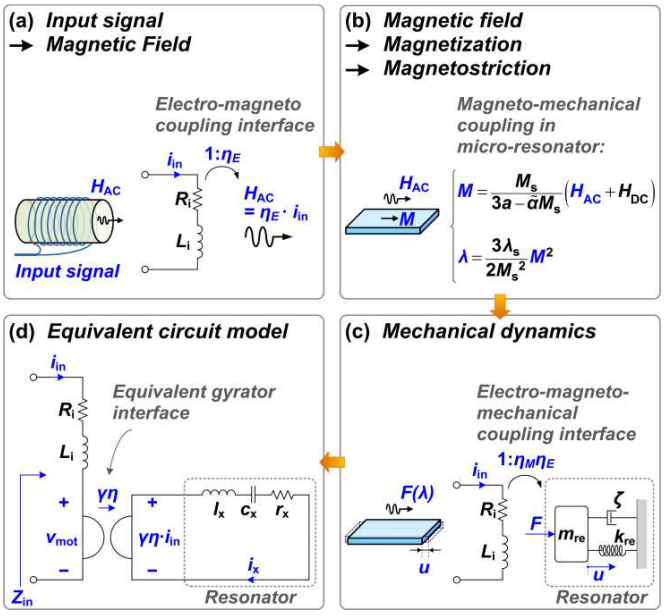

Fig. 3 Modeling route for establishment of the equivalent circuit for the mass-sensing ME-resonator.

Equivalent-circuit modeling of ME μ-diver

For systematic analysis of the MER-μDS, we develop a novel modeling method for the ME μ-diver, which includes four steps to build a complete equivalent circuit model, as is shown in Fig. 3.

Step (a): Shown in Fig. 3(a) is the coil coupling interface modeling for the excitation magnetic field of H_{AC}, herein

$$H_{\text{AC}} = \eta_E \cdot i_{\text{in}} = \frac{N}{2\sqrt{r^2 + l^2/4}} \cdot i_{\text{in}} \quad (3)$$

where η_E is defined as electro-magneto coupling coefficient; i_{in} is the input signal; N, r and l are the number of turns, inner radius and length of the coil, respectively.

Step (b): Shown in Fig. 3(b) is the magnetization modeling of the μ-diver ME material for the magnetism M and magneto-striction λ from H_{AC}. Since ME materials commonly have very low coercivity. With hysteresis effect ignored, the M–H relation is given as[31]

$$M = M_s\left[\coth\left(\frac{H_{eff}}{a}\right) - \frac{a}{H_{eff}}\right] \approx \frac{M_s H_{eff}}{3a}, \quad (H_{eff} << a) \quad (4)$$

where H_{eff} is the effective magnetic field in the resonator that is mainly determined by $H_{\text{DC}}+H_{\text{AC}}+\tilde{\alpha}M$. Herein $\tilde{\alpha}M$ denotes the field form the magnetic interaction between the moments, with the parameter $\tilde{\alpha}$ quantifying the amount of inter-domain interaction and can be experimentally determined for a concrete system. Herein M_s is the saturation magnetization of the ME material. a equals to $Nk_BT/(\mu_0 M_s)$, where N is the domain density, k_B is the Boltzmann constant, T is temperature and μ_0 is permeability in air.

Assuming the magnetic moments being originally perpendicular to the applied field, the corresponding magneto-striction λ is

$$\lambda = \frac{3\lambda_s}{2M_s^2} M^2 = \frac{3\lambda_s}{\left(3a - \tilde{\alpha} M_s\right)^2} H_{\text{DC}} H_{\text{AC}} \quad (5)$$

where λ_s is the saturation magneto-striction. In Eq. (5), only the λ-component at the fundamental-mode frequency is picked for following small-signal equivalent-circuit modeling.

Step (c): The modeling shown in Fig. 3(c) is to build mechanical dynamics of the resonator with the λ induced excitation force. Taking the ME bar in the longitudinal bulk resonance-mode as example, where the magnetostriction along the longitudinal direction and damping effect are taken into consideration, the corresponding wave-equation is [32-34]

$$\rho A \frac{\partial^2 U}{\partial t^2} = \frac{EA}{1-\nu^2}\frac{\partial^2 U}{\partial x^2} - EA\frac{\partial \lambda}{\partial x} + c_{\text{D}} A \frac{\partial^3 U}{\partial x^2 \partial t} - \frac{2\eta_{\text{liq}}\beta A \cdot \text{Re}\left[\kappa \cot(\kappa h)\right]}{\rho d} \cdot \frac{\partial U}{\partial t} \quad (6)$$

where U is the vibration displacement as a function of time and position, ρ denotes material density, d is thickness of the resonator structure, c_{D} is material damping, h is the equivalent liquid depth at each side of the resonating plane, κ equals to $(1+j)/\delta$ with j as the complex number and $\delta=[\eta_{\text{liq}}\cdot(\pi\rho_{\text{liq}}f_{\text{air}})^{-1}]^{1/2}$ expressing the penetration depth of the wave into liquid, β is a ratio related to surface roughness, A is cross-sectional area of the μ-diver. Herein the ΔE-effect is neglected. By applying standing wave solution form of $U=u(t)\cdot\sin(\pi x/L)$ and integrating over the length in Eq. (6), the mechanic dynamics model can be obtained as

Lab on a Chip Accepted Manuscript

$$\frac{\rho AL}{2}\cdot\frac{\partial^2 u}{\partial t^2}+\left\{\frac{\pi^2 A}{2L}c_D+\frac{\eta_{\text{liq}}\beta AL}{\rho d}\cdot\text{Re}\left[\kappa\cot(\kappa h)\right]\right\}\frac{\partial u}{\partial t}+\frac{\pi^2 EA}{2L(1-\nu^2)}u=-2EA\lambda \quad (7)$$

Eq. (7) indicates that the resonation is excited by the magneto-striction induced elastic force of $2EA\lambda$ (herein the minus sign is ignored without altering frequency domain results) as

$$F=2EA\lambda=\frac{6\lambda_s EA\cdot H_{DC}}{(3a-\tilde{\alpha}M_s)^2}H_{AC}=\eta_M\cdot H_{AC} \quad (8)$$

where η_M is defined as magneto-mechanical coupling coefficient. By defining effective mass m_{re}, damping ζ and stiffness k_{re}, Eq. (7) is then converted to a more general form of

$$m_{\text{re}}\cdot\frac{\partial^2 u}{\partial t^2}+\zeta\cdot\frac{\partial u}{\partial t}+k_{\text{re}}\cdot u=F \quad (9)$$

Table 1 summarizes the calculated k_{re} and m_{re} of the three resonance modes of our considered three types of μ-diver structures, respectively. Herein the mass loading effect from the liquid is relatively weak enough and, thus, ignored.

Step (d): As is shown in Fig. 3(d), this step is employed to establish the full equivalent-circuit model. With input signal as $\gamma\eta\cdot i_{\text{in}}$ and motional current as i_{x}, Eq. (9) is further converted into vibration equation of $r_{\text{x}}l_{\text{x}}c_{\text{x}}$ series circuit as

$$l_{\text{x}}\frac{di_{\text{x}}}{dt}+r_{\text{x}}i_{\text{x}}+\frac{1}{c_{\text{x}}}\int i_{\text{x}}dt=\gamma\eta\cdot i_{\text{in}} \quad (10)$$

Herein

$$\begin{cases}\eta=\eta_M\eta_E,\\ l_{\text{x}}=\gamma^2 m_{\text{re}},\ r_{\text{x}}=\gamma^2\zeta,\ c_{\text{x}}=1/\left(\gamma^2 k_{\text{re}}\right)\\ \gamma=1\ \text{m/C (unit converter)}.\end{cases} \quad (11)$$

and η is defined as an electro-magneto-mechanical coupling coefficient that expresses the energy coupled from electric source to mechanical vibration of the ME resonator. The obtained equivalent circuit model of the system is given in Fig. 3(d), with an ideal transformer acting as the energy-coupling component. Considering the electric signal relationship between double sides of the transformer, the equivalent circuit can be further simplified by removing the transformer and combining the excitation and the resonator branches in parallel. Fig. 4 shows the simplified circuit model that is composed of following elements of

$$\begin{cases}L_x=m_{re}\eta^{-2} & \text{(motional inductance)}\\ R_x=\zeta\eta^{-2} & \text{(motional resistance)}\\ C_x=\eta^2 k_{re}^{-1} & \text{(motional capacitance)}\end{cases} \quad (12)$$

Finally, the reflection coefficient s_{11} to be measured is given by

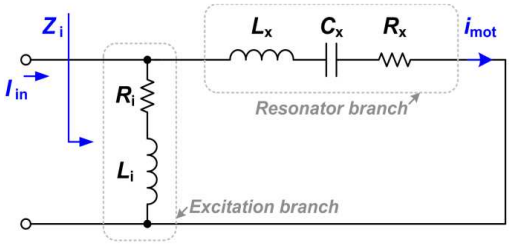

Fig. 4 Simplified equivalent circuit model for the wireless sensor.

$$s_{11}=\left(Z_{\text{i}}-Z_0\right)/\left(Z_{\text{i}}+Z_0\right) \quad (13)$$

where Z_{i} is the input impedance of the equivalent circuit and Z_0 is the characteristic impedance of the network analyzer.

Table 1 Resonance-mode design for different resonator structures [36-38]

	Bar, in longitudinal mode [36]	Square-plate, in Lamé mode [37]	Disk, in wine-glass mode [38]
Mode-shapes of different structures	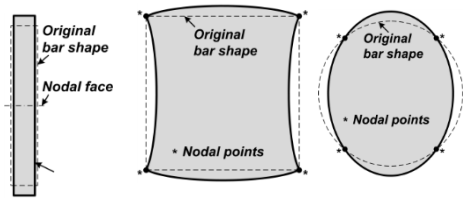		
m_{re}	$0.5m_0$	$0.5m_0$	$0.21m_0$
k_{re}	$\frac{4.93EA}{L(1-\nu^2)}$	$9.87Gd$ (G: shear modulus)	$\frac{1.35Ed}{1-\nu^2}$ *

* Diameter equals to 21d.

Experiments

Fabrication of ME micro-resonators

Commercially available ME material (Metglas®2826MB or Vitrovac®7600 T70) in ribbon form is used to fabricate the ME resonators. Metglas®2826MB is received in the form of rolls of ribbon with width as 12.5mm and thickness as 25μm. Differently, Vitrovac®7600 T70 is with the width as 20mm and the thickness as 20μm. The pieces of the ME-material are ultrasonically washed with ethanol for 2 min. In order to implement antibody immobilization on the resonator surface and to further protect the ME-material from degradation in saline solution, a composite thin-film of 500nm-thick gold on 50nm-thick chromium is deposited onto both sides of the ME film by sputtering with a Denton@ Discovery-24 multi-target magnetic control sputtering system. The chromium layer serves as adhesive interlayer between the top-side gold layer and the ME film.

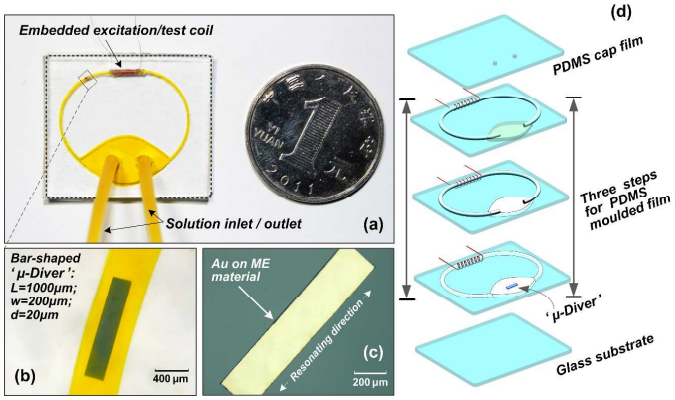

Fig. 5 (a) Top-view photo-graph of the fabricated MER-μDS chip. (b) Close-up viewed micro-graph of the bar-shaped ME resonant μ-diver assembled in the micro-fluidic channel. (c) Micro-graph showing the μ-diver, with one surface coated with 500nm-thick Au thin-film for the following bio-probe immobilization. (d) Schematic micro-assembly process steps for the formation of the MER-μDS chip.

Lab on a Chip Accepted Manuscript

This journal is © The Royal Society of Chemistry 2014

Then the material is saw diced into rectangular micro-bars, with two different dimensions of 2000μm×400μm and 1000μm×200μm. After cleaned, the ME resonating bars are annealed to relieve the internal residual stress and eliminate the defects due to saw dicing. The annealing is processed at 250°C for 2hrs in a nitrogen filled furnace.[35] Then, the samples are slowly cooled down to room temperature in the nitrogen filled environment.

Fabrication of microfluidic system

For the formation of the MER-μDS, the micro-assembling process starts from a polydimethylsiloxane (PDMS) cap film. The PDMS is purchased from ABCR. The micro-fabricated microsystem consists of a PDMS film with moulded microfluidic structures, a copper micro-coil, a glass-substrate and a length extentional-mode resonant μ-diver made of amorphous ME alloy (e.g., Vitrovac®7600 T70 or Metglas®2826MB), as is shown in Fig. 5. The PDMS cap film (30mm×25mm×1.5mm) is made in a preformed plastic mould, with two holes opened to the connect inlet/outlet tubes. Then, three process steps are implemented to make the moulded film. At the first step, a micro-channel model for shaping the micro-channel and a micro-cavity mould for the bio-reaction chamber are immersed in the middle PDMS film. In fact the micro-channel mould is a soft fishing line (diameter = 0.5mm), around which the metal micro-coil was previously wound. At the second step, the micro-cavity for the bio-reaction chamber mould is picked after the PDMS is solidified in room-temperature. At the third step, the fishing line is pulled out carefully. In this way the micro-fluidic channel is formed and the micro-coil is still remained in the designed location of the channel. The process details are shown in Fig. 5(d). A 1mm-thick glass substrate is used as bottom plate to hold the PDMS micro-chip. After plasma pre-treatment is implemented to the double surfaces to be bonded, the three parts of the chip are assembled together by bonding process. Before the binding step, the micro-resonator was already put in the bio-reaction chamber.

Detection of magnetic-beads for sensitivity calibration

Used in sensing experiment, commercially available Dynabeads®M-270 Streptavidin is purchased from Invitrogen, and the EZ-Link™ Sulfo-NHS-SS-Biotin (sulfosuccinimidyl-2-biotinamido-ethyl-1,3-dithiopropionate) kit is bought from Thermo Scientific. The initial concentration of the Dynabeads®M-270 Streptavidin is 10mg mL^{-1} (in 0.0065M phosphate buffer, pH=7.4), with 0.14M NaCl and 0.02% sodium azide as preservative. The Sulfo-NHS-SS-Biotin is a kind of thiol-cleavable amine-reactive biotinylation reagent that contains extended spacer arm to reduce avidin-binding associated steric hindrance. In order to refresh the surface of the ME resonator, the μ-diver is ultrasonically pretreated in ethanol for 2 min and, then, cleaned with deionized (DI) water. Before bonding the micro-channel molded PDMS chip with the glass substrate, the cleaned resonator is put in the bio-reaction chamber. After the binding, 0.1 M phosphate buffered saline (PBS) solution (containing 2.5 mM sulfo-NHS-SS-biotin) is pumped into the chamber. Then, the microfluidic system is placed in a fridge at 4°C for 8 hrs. Thereafter, the thiolated biotin species and ω-mercapto propionic acid are modified on the gold surface of the ME resonator to form mixed self-assembled monolayers (SAMs). Herein the PBS solution with pH=7.0 is prepared with KH_2PO_4 and NaOH. During the process, the N-hydroxysulfosuccinimide portion in the Sulfo-NHSSS-biotin is easily hydrolyzed by water.

After the surface modification, the resonator is rinsed sequentially with ethanol, DI water and PBS solution in the chamber. Then the magnetic-bead solution (with 10^6 beads mL^{-1} concentration) is flown through the MER-μDS for biotin-avidin binding, while an Agilent-E5072A network analyzer is used to real-time record the frequency. By counting the number of the beads (with known mass of 15pg per bead) that are bound at the μ-diver surface, the total mass change can be worked out. With the recorded resonant frequency shift, the mass sensitivity of the sensor can be calculated according to Eq. (2).What's more, another μ-diver without surface modification as a control sensor is also measured in the magnetic-bead solution with 10^6 beads mL^{-1} concentration. Control sensors are applied in this study to compensate for the non-specific binding and environmental changes.

Direct liquid-phase detection of *E. coli* bacteria

By specific binding of *E. coli* bacteria with pre-immobilized anti-*E. coli* polyclonal antibody (pAb), the increase in effective mass of the resonator causes a corresponding decrease of the resonant frequency. The anti-*E. coli* polyclonal antibody sample is purchased from Pierce Rockford. Bovine serum albumin (BSA) and avidin are purchased from Sigma-Aldrich. The sample of *E. coli* is cultured in our own laboratory. As is described in last sub-section, the thiolated biotin species are modified on the Au surface of the resonator with similar process. Thereafter, avidin modification on the biotinylated resonator is implemented by incubating the resonator in a 0.3 mg mL^{-1} avidin contained PBS solution for more than 30 min in the chamber. By net positive charge carrying effect that is originated from its 10.5 isoelectric point (pI), the avidin is electrically attracted to the mixed SAM and, thus, immobilized on the resonator via biotin-avidin interaction. Then 0.3mg mL^{-1} of the biotinylated antibody is introduced to the chamber for 1 hr to complete the antibody immobilization. After 1% BSA is injected for 1 hr to passivate the unspecific sites, the pAb functionalized μ-diver is well prepared in the MER-μDS for online biological detection. With the *E. coli* bacteria sample flows through the MER-μDS chip for 10 min, the generated Δf signal of the ME resonant μ-diver is wirelessly picked up by the coil and analyzed by using network analyzer. For obtaining uniform sensing data, the Δf signal at the end of the tenth minute is always recorded. To compensate for environmental and non-specific binding effects, control sensors are prepared following the same steps but without antibody immobilized.

For pathogen detection in real liquid food, the *E. coli* bacteria are added into commercial apple juice and orange juice (purchased from supermarket, Hui-Yuan brand), respectively, to prepare the samples of varied pathogen concentrations. Then the liquid-food samples are introduced into the MER-μDS chip for detection.

Results and Discussion

Experimental validation of the equivalent-circuit design model

Experimentally, the resonance peaks of the μ-diver in air and liquid solution environments are wirelessly detected, respectively, by using the coil. For in-air measurement, there is no liquid in the channel. In contrast, the resonator swims along

Lab on a Chip Accepted Manuscript

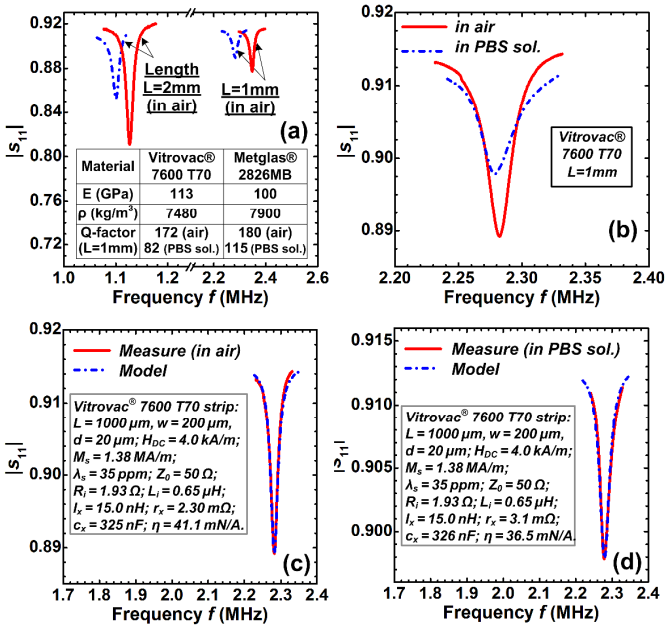

Fig. 6 (a) Measured resonance peaks of the bar-shaped micro-resonators made of Metglas® 2826MB (in blue dash lines) and Vitrovac® 7600 T70 (in red solid lines) the resonators with 1mm and 2mm in length are respectively tested, with the tested Q values compared in the inset table.(b) The micro-resonators made of Vitrovac® 7600 T70 with 1mm in length are tested in air (red solid line) and in PBS solution (blue dash line). (c) Parameter extraction by using the equivalent circuit model (blue dash line) that agrees well with the measurement (red solid line). Herein the 1mm-long Vitrovac® 7600 T70 ME-resonator is tested in air.(d) Herein the 1mm-long Vitrovac® 7600 T70 ME-resonator is tested in PBS solution.Parameter extraction by using the equivalent circuit model (blue dash line) that also agrees well with the measurement (red solid line).

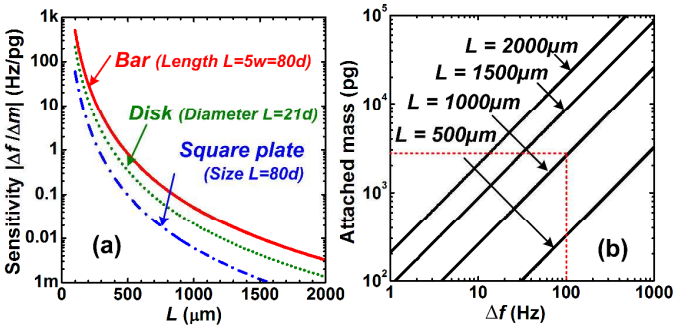

Fig. 7 (a) Analyzed results suggest that the bar-shaped ME resonator has the highest mass sensitivity among the three shapes of resonant structures listed in Table 1. (b) Theoretically obtained ***Δm~Δf*** relationship for the bar-shaped resonator with varied structural length. Note: herein the resonators are made of the ME-material of Vitrovac® 7600 T70 in PBS solution.

the PBS solution filled channel to the coil located position for resonance excitation and signal readout. With the frequency-domain testing results shown in Fig. 6(a), the bar-shaped micro-resonators (with different lengths) made of Metglas®2826MB and Vitrovac®7600 T70 are measured in air, respectively. As is listed in the inset table, the in-air Q-factor values of the two ME materials are generally similar. As for the test in PBS solution, Metglas®2826MB shows a bit higher Q-factor compared to Vitrovac®7600 T70. The deviation of resonant frequency from different materials but identical geometries is induced by difference in material density and Young's modulus. In Fig. 6(b), The micro-resonators made of Vitrovac® 7600 T70 with 1mm in length are tested in air (red solid line) and in PBS solution (blue dash line). Compared with the resonant frequency in air, there's a frequency shift in PBS solution as Eq. (1) indicated. In Fig.6 (c) and (d), the micro-resonators made of Vitrovac® 7600 T70 with 1mm in length are tested in air and in PBS solution. The red solid lines shows the measured resonance peak and the blue dash lines represents the characteristic extracted from the equivalent-circuit model. Obviously, the measured resonance-peak matches very well with the modeling prediction in terms of both resonance-peak shape and S_{11} parameter, thereby well validating the accuracy of our established model for design of the resonant sensor.

Fig. 7(a) compares the calculated mass sensitivities of the various ME-resonator structures listed in Table I in air, which are the bar-shaped structure in longitudinal extension mode, the square-plate structure in Lamé mode and the disk-shaped structure in wine-glass resonance mode. If identical structural length of L is assumed for all the three resonators, the calculated results indicate that the bar-shaped resonator exhibits the highest sensitivity [see Fig. 7(a)], thereby being selected as the sensor for experiment. According to Eq. (1), resonant frequency of the bar-shaped resonator is only dependent of its length. Fig. 7(b) shows the calculated relation between the adsorbed mass and the frequency shift for various bar lengths in PBS solution. Given a noise-floor limited minimum readable frequency-shift, apparently a smaller detectable mass benefits from a shorter bar length. With our currently fabricated MER-μDS chip, wireless detection signal for the resonant bars of shorter than 1000μm is too weak to be reliably read out. Therefore, the 1000μm-long μ-divers are used in our sensing experiments. Corresponding to the noise restricted frequency signal of tens of Hz, the mass detecting resolution is estimated as about several hundreds of picogram.

As for material selection between Metglas®2826MB and Vitrovac®7600 T70, the latter made resonant bar demonstrates similar Q value in air to the former made device, but shows a bit

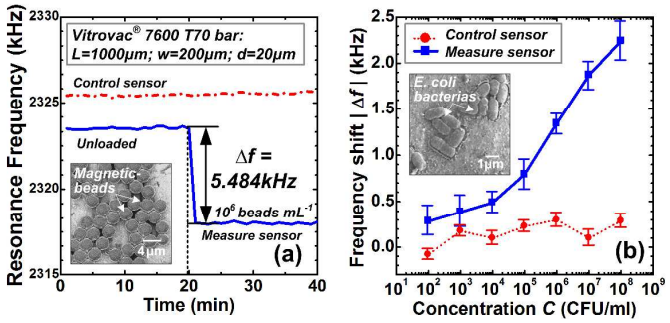

Fig. 8 (a) Real-time measured resonance-frequency signals of the control sensor (red line) and the measure sensor (blue line) to detect magnetic-bead solution for mass sensitivity calibration. (b) Wirelessly recorded ***Δf*** of the control sensor (red dash line) and the measure sensor (blue solid line) through different *E. coli* concentrations in PBS buffer solution. The Insets of the two figures show the beads and the *E. coli* bound on the surface of the resonators, respectively.

Lab on a Chip Accepted Manuscript

This journal is © The Royal Society of Chemistry 2014

lower Q in solution. However, the available latter material sheet is thicker than the former that is favorable for higher frequency-shift signal [see Eq. (2), thicker resonant bar has larger mass M]. The higher E/ρ ratio of the latter material helps to gain higher resonance frequency [see Fig. 6(a)]. Thus, the μ-divers made of Vitrovac®7600 T70 are optimally selected for bio-sensing experiment.

Biological detection results

After the bar-shaped resonator is with biotin modified on its gold surface, it is put in the MER-μDS and exposed to the flow of the streptavidin attached magnetic-beads. The ME-resonator used in this experiment is made of Vitrovac® 7600 T70 and with the length, width and thickness as 1000μm, 200μm and 20μm. As is expected, the real-time resonance-frequency signals of the control sensor (red line) and the measure sensor (blue line) are wirelessly read out and recorded in Fig. 8(a). The inset SEM image in the figure demonstrates the beads adsorbed on the resonator surface by biotin-avidin interaction. When 10^6 beads mL^{-1} concentration magnetic-bead solution is used for detection, 5.484kHz frequency-shift is measured that is induced by the attached bead mass of about 90 ng. The 90 ng additional mass is obtained by counting the attached bead number of about 6000 under a microscope. The averaged mass per bead is known as 15pg. Therefore, the mass sensitivity is experimentally obtained as about 0.061Hz pg^{-1}. This result generally agrees with the theoretically calculated sensitivity of 0.040 Hz pg^{-1} [see Fig. 7(b)].

In the biological detection for *E. coli* bacteria, the antibody was pre-immobilized on the ME-resonator, which has identical structure to the bead-measurement used one. In Fig. 8(b), the Δf sensing signals of the control sensor (in red dash line) and the measure sensor (with antibody immobilized, in blue solid line) are recorded together. All the data points are the averaged results for three-time detection. Error bar is shown for each test point. Corresponding to the bacterial samples flowing into the MER-μDS where the concentration is sequentially increased from 10^2 to 10^8 CFU mL^{-1}, the Δf sensing signals of the measure sensor from about 300 Hz to 2300 Hz are wirelessly picked up by the coil and online recorded. As is shown in the inset SEM image of Fig. 8(b), adsorption of *E. coli* bacteria on the μ-diver is via specific interaction with the antibody. The minimum detectable concentration is about 100 CFU/mL.

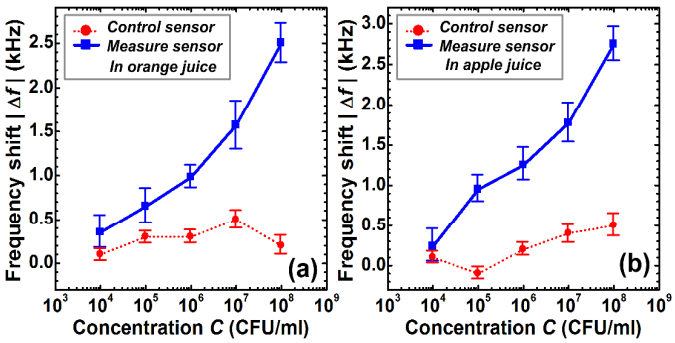

Fig. 9 (a) Wirelessly recorded Δf signals for the measure sensor (blue solid line) and the control sensor (red dash line) to detect the orange juice samples with varied *E. coli* concentrations, respectively. (b) Detected Δf for the measure and control sensors to detect the *E. coli* added apple juice samples.

The control experimental results for both the magneto-beads detection and the pathogen bio-sensing are plotted in Figs. 8(a) and 8(b) for comparison. In Fig. 8(a), the resonance frequency of the control sensor without surface modification has no obvious change as time goes on. In Fig. 8(b), the control sensor without the antibody immobilized on the sensor surface, non-specific adsorption induced frequency-shift is generally within ±0.25 kHz that is lower than the specific sensing response for the minimum detectable *E. coli* concentration of 10^2 CFU ml^{-1}. In addition, the non-specifically adsorbed mass increase along with increase of the pathogen concentration is not noticeable.

In fact, our anticipated minimum detectable concentration is 10 CFU mL^{-1}. In order to realize the sensing performance in near future, the mass sensitivity should be enhanced by decreasing the length of the ME resonant μ-driver. Accordingly, better microfluidic chips with thinner micro-channel and more turns of the coil should be micro-fabricated to reliably read out the weaker ME resonating signals.

In order to examine bio-detection performance of the ME resonant micro-system for real liquid food, the *E. coli* pathogens are added into commercial apple juice and orange juice, respectively, to form the samples of varied *E. coli* concentrations. The sensing results together with the control experiments are shown in Fig. 9. With the *E. coli* concentration sequentially increased from 10^4 to 10^8 CFU mL^{-1}, the bacterial fruit juice flows into the MER-μDS and the corresponding Δf sensing signal is wirelessly picked up by the coil and online recorded. The results in Fig. 9 preliminarily prove the application feasibility of the MER-μDS technique in real liquid food. The detection sensitivity for the fruit juice is similar to that for PBS solution. However, merged in the more sticky fruit juice, the ME resonator exhibits lower Q-factor and smaller resonating amplitude. The weaker resonance leads to lower signal/noise ratio and worse limit of detection (herein about 10^4 CFU mL^{-1}) compared to that for PBS aqueous solution (about 10^2 CFU mL^{-1}). Our future work will be focused on further improvement of the minimum detectable pathogen concentration in viscous liquid food.

Conclusions

A LOC type magneto-elastic (ME) resonant μ-diver system (MER-μDS) is proposed and prototyped, which features three novelties of: (1) integrated microfluidic platform with repeatedly usable magneto-elastic micro-resonator (namely μ-diver); (2) rapid operation mode for in-liquid pathogen detection with micro-coil wireless signal readout; (3) the built equivalent-circuit modeling method for design of the resonant ME-bar towards ultra-sensitive bio-sensing applications. Bar-shaped resonant 'μ-diver' with longitudinal extension-mode has been optimally designed and micro-fabricated. Then the MER-μDS fluidic chip is formed by micro-machining and micro-assembling techniques. By using the biotin pre-functionalized MER-μDS, the experiment for detection of avidin-modified magnetic-beads (with concentration of 10^6 beads mL^{-1}) is carried out to obtain the mass detection sensitivity of 0.061Hz pg^{-1}. Then the experiment for detection of *E. coli* bacteria is implemented with the antibody pre-immobilized μ-diver. Corresponding to the *E. coli* PBS-solution of 10^2~10^8 CFU mL^{-1}, about 300~2300 Hz f_0-shift

Lab on a Chip Accepted Manuscript

sensing-signals are wirelessly picked up. Therefore, the microfluidic system of MER-μDS is very promising for on-site and real-time wireless detection of pathogens in liquids.

Acknowledgements

This study is supported by NSF of China (91323304, 61234007, 61321492, 51405480), Chinese 973 Project (2011CB309503), National Key Technology R&D Program (2012BAK08B05) and Science and Technology Commission of Shanghai Municipality grant (11391901900).

References

1 G. M. Whitesides, *Nature*, 2006, **442**, 368–373.
2 P. Yager, T. Edwards, E. Fu, K. Helton, K. Nelson, M. R. Tam and B. H. Weigl, *Nature*, 2006, **442**, 412–418.
3 S. Neethirajan, I. Kobayashi, M. Nakajima, D. Wu, S. Nandagopal and F. Lin, *Lab Chip*, 2011, **11**, 1574-1586.
4 S. Bouguelia, Y. Roupioz, S. Slimani, L. Mondani, M. G. Casabona, C. Durmort, T. Vernet, R. Calemczuk and T. Livache, *Lab Chip*, 2013, **13**, 4024-4032.
5 J. Zhang, S. Liu, P. Yang and G. Sui, *Lab Chip*, 2011, **11**, 3516-3522.
6 P. Neuzil, L. Novak, J. Pipper, S. Lee, L. F. P. Ngxb and C. Zhang, *Lab Chip*, 2010, **10**, 2632-2634.
7 V. Velusamy, K. Arshak, O. Korostynska, K. Oliwa and C. Adley, *Biotechnol. Adv.*, 2010, **28**, 232–254.
8 A. M. Valadez, C. A. Lana, S. Tu, M. T. Morgan and A. K. Bhunia, *Sensors*, 2009, **9**, 5810-5824.
9 T. Fukuba, Y. Aoki, N. Fukuzawa, T. Yamamoto, M. Kyoe and T. Fujii, *Lab Chip*, 2011, **11**, 3508-3515.
10 C. D. Chin, V. Linderb and S. K. Sia, *Lab Chip*, 2007, **7**, 41-57.
11 R. Damadian, *Science*, 1971, **171**, 1151-1153.
12 S. Miltenyi, W. Muller, W. Weichel and A. Radbruch, *Cytometry*, 1990, **11**, 231-238.
13 M. Shao, F. Ning, J. Zhao, M. Wei, D. G. Evans and X. Duan, *J. Amer. Chem. Soc.*, 2012, **134**, 1071-1077.
14 J. Do and C. H. Ahn, *Lab Chip*, 2008, **8**, 542-549.
15 R. Abbundi and A. E. Clark, *J. Appl. Phys*., 1978, **49**, 1969-1971.
16 E. A. Lindgren, S. Haroush, J. C. Poret, A. D. Mazzatesta, M. Rosen, M. Wun-Fogle, J. B. Restorff, A. E. Clark and J. F. Lindberg, *J. Appl. Phys*., 1998, **83**, 7282-7284.
17 M. B. Moffett, A. E. Clark, M. Wun-Fogle, J. Linberg, J. P. Teter and E. A. McLaughlin, *J. Acoust. Soc. Am.*,1991, **89**, 1448-1455.
18 F. Claeyssen, N. Lhermet, R. L. Letty and P. Bouchilloux, *J. Alloys Compd.*, 1997, **258**, 61-73.
19 R. Guntupalli, J. Hu, R. S. Lakshmanan, T. S. Huang, J. M. Barbaree, and B. A. Chin, *Biosens. Bioelectron.,* 2007*,* **22**, 1474-1479.
20 W. Shen, L. C. Mathison, V. A. Petrenko, and B. A. Chin, *J. Phys. D: Appl. Phys.,* 2010*,* **43**, 015004.
21 X. L. Su and Y. Li, *Biosens. Bioelectron.,* 2005, **21**, 840-848.
22 Y. H. Chang,H. D. Jang, C. L. Hsu and K. S. Chang, *Analytical Letters*, 2012, **45**, 1485-1494.
23 E. Howe and G. Harding, *Biosens. Bioelectron.,*2000, **15**, 641-649.
24 R. Hao, D. Wang, X. Zhang, G. Zuo, H. Wei, R. Yang, Z. Zhang, Z. Cheng, Y. Guo, Z. Cui and Y. Zhou, *Biosens. Bioelectron.*, 2009, **24**, 1330–1335.
25 R. Z. Hao, H. B. Song, G. M. Zuo, R. F. Yang, H. P. Wei, D. B. Wang, Z. Q. Cui, Z. Zhang, Z. X. Cheng and X. E. Zhang, *Biosens. Bioelectron.*, 2011, **26**, 3398–3404.
26 X. X. Li and D. W. Lee, *Meas. Sci. Technol.*, 2012, **23**,0957-0233.
27 T. Xu, H. Yu, P. Xu and X. X. Li, *Biomed. Microdevices*, 2012, **14**, 303–311.
28 Y. H. Tao, X. X. Li, T. G. Xu, H. T. Yu, P. C. Xu, B. Xiong and C. Z. Wei, *Sens. Actuators*, B, 2011, **157**, 606–614.
29 M. Ramasamy and C. Liang, *SEM Annual Conference,* 2010, **2**, 9-15.
30 P. G. Stoyanov and Craig A. Grimes, *Sensors and Actuators A: Physical,* 2000, **80**, 8-14.
31 M. J. Dapino, R. C. Smith, and A. B. Flatau, *IEEE Trans. Magn.,* 2000, **36**, 545-556.
32 S. J. Martin, J. J. Spates, K. O. Wessendorf, T. W. Schneider, and R. J. Huber, *Anal. Chem.,*1997, **69**, 2050-2054.
33 P. G. Stoyanov and C. A. Grimes, *Actuators A*, 2000, **80**, 8-14.
34 X. Zheng and L. Sun, *J. Magn. Magn. Mater.*, 2007, **309**, 263–271.
35 S. Huang, J.Hu and B. A. chin, *Materials Science and Engineering*, 2008, **28**, 380-386.
36 L. D. Landau and E. M. Lifshitz, *Theory of Elasticity* 3rd, 1986, **7**, 46-49.
37 J. E. -Y. Lee, J. Yan, and A. A. Seshia, *J. Micromech. Microeng.*, 2009, **19**, 074003.
38 Y. -W. Lin, S. Lee, S. -S. Li, Y. Xie, Z. Ren, and C. T. -C. Nguyen, *IEEE J. Solid-State Circ.*, 2004, **39**, 2477-2491.

Lab on a Chip Accepted Manuscript

 This journal is © The Royal Society of Chemistry 2014